

Observational approaches to understanding dark energy

Yun Wang

Homer L. Dodge Department of Physics & Astronomy, Univ. of Oklahoma,
440 W. Brooks St., Norman, OK 73019, USA; wang@nhn.ou.edu

Illuminating the nature of dark energy is one of the most important challenges in cosmology today. In this review I discuss several promising observational approaches to understanding dark energy, in the context of the recommendations by the U.S. Dark Energy Task Force and the ESA-ESO Working Group on Fundamental Cosmology.

I. INTRODUCTION

The discovery that the expansion of the universe is accelerating today was first made in 1998 [1, 2]. The evidence for the cosmic acceleration has strengthened over time. Illuminating the nature of dark energy is one of the most exciting challenges in cosmology today.

The expansion history of the universe is described by the Hubble parameter, $H(t) = (d \ln a / dt) = \dot{a} / a$, where $a(t)$ is the cosmic scale factor, and t is cosmic time. The cosmological redshift, $z \equiv 1/a(t) - 1$, is usually used as the indicator for cosmic time, because it can be measured for a given astrophysical object. Fig.1 shows the Hubble parameter $H(z)$, as well as \dot{a} , measured from current observational data [3].

The observed cosmic acceleration could be due to an unknown energy component (dark energy, *e.g.*, [8]), or a modification to general relativity (modified gravity, *e.g.*,

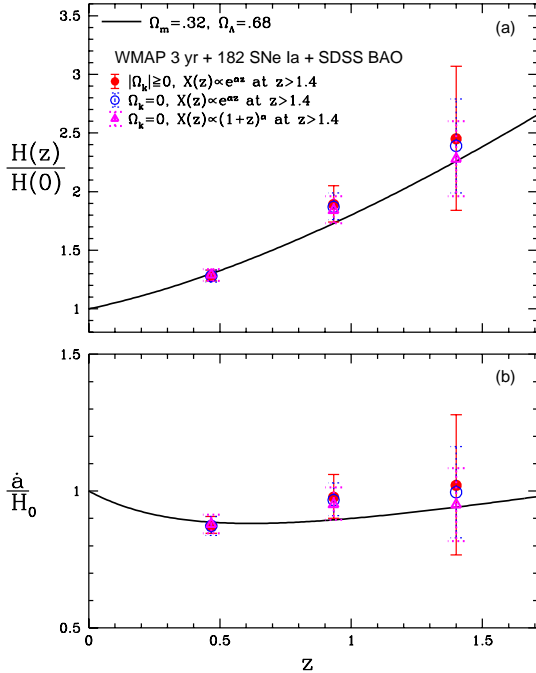


FIG. 1: Expansion history of the universe measured from current data [3]. Data used: Cosmic microwave background anisotropy (CMB) data from WMAP 3 year observations [4]; 182 Type Ia supernovae (SNe Ia) (compiled by [5], including data from the Hubble Space Telescope (HST) [5], the Supernova Legacy Survey (SNLS) [6], as well as nearby SNe Ia); Sloan Digital Sky Survey (SDSS) baryon acoustic oscillation measurement [7]. Note that $X(z) \equiv \rho_X(z)/\rho_X(0)$ in the figure legends.

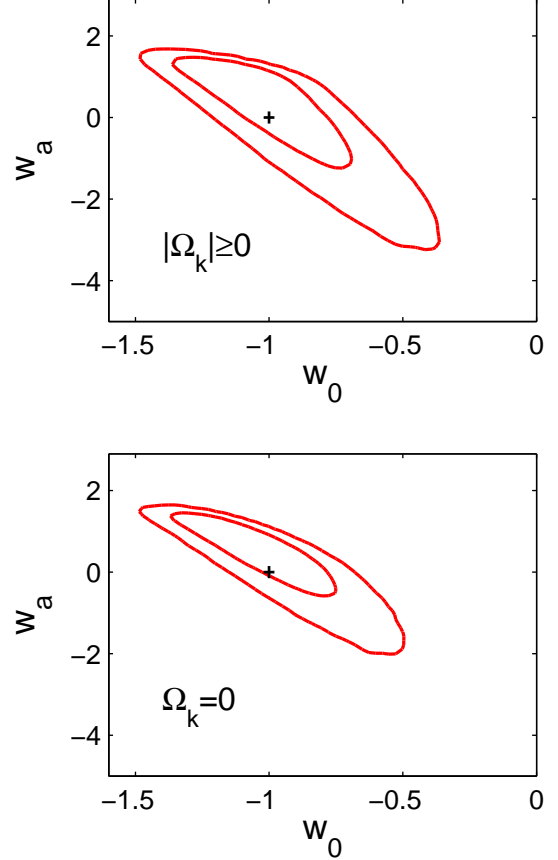


FIG. 2: Constraints on the dark energy equation of state $w_X(a) = w_0 + w_a(1-a)$ [14] using the same data as in Fig.1. A cosmological constant corresponds to $w_X(a) = -1$ (indicated by the cross in the figures). [3]

[9, 10]). Ref.[11] contains reviews with more complete lists of references of theoretical models.

The simplest explanation for the observed cosmic acceleration is that dark energy is a cosmological constant (although it is many orders smaller than expected based on known physics), and that gravity is not modified. Fig.1 and Fig.2 show that a cosmological constant is consistent with current observational data, although uncertainties are large. For complementary approaches to analyzing current data, see, *e.g.*, [12, 13].

I will discuss the general guidelines for dark energy search in Sec.2, several promising observational methods in Sec.3, and conclude with a summary of current status and future prospects of dark energy experiments in Sec.4.

II. GENERAL GUIDELINES FOR DARK ENERGY SEARCH

There are two fundamental questions that need to be answered by dark energy search:

- (1) Is dark energy density constant in cosmic time?
- (2) Is gravity modified?

These questions can be answered by the precise and accurate measurement of the dark energy density $\rho_X(z)$ as a function of cosmic time [or the expansion history of the universe, $H(z)$, see Eq.(2)], and the growth history of cosmic large scale structure, $f_g(z)$ [see Eqs.(3) and (4)], from observational data.

Dark energy is often parameterized by a linear equation of state $w_X(a) = w_0 + w_a(1 - a)$ [14]. Because of our ignorance of the nature of dark energy, it is important to make model-independent constraints by measuring the dark energy density $\rho_X(z)$ [or the expansion history $H(z)$] as a free function of cosmic time. Measuring $\rho_X(z)$ has advantages over measuring dark energy equation of state $w_X(z)$ as a free function; $\rho_X(z)$ is more closely related to observables, hence is more tightly constrained for the same number of redshift bins used [15, 16, 17]. Note that $\rho_X(z)$ is related to $w_X(z)$ as follows [15]:

$$\frac{\rho_X(z)}{\rho_X(0)} = \exp \left\{ \int_0^z dz' \frac{3[1 + w_X(z')]}{1 + z'} \right\}, \quad (1)$$

Hence parametrizing dark energy with $w_X(z)$ implicitly assumes that $\rho_X(z)$ does not change sign in cosmic time. This precludes whole classes of dark energy models in which $\rho_X(z)$ becomes negative in the future (“Big Crunch” models, see [18] for an example)[19].

If the present cosmic acceleration is caused by dark energy,

$$E(z) \equiv \frac{H(z)}{H_0} = [\Omega_m(1+z)^3 + \Omega_k(1+z)^2 + \Omega_X X(z)]^{1/2}, \quad (2)$$

where $X(z) \equiv \rho_X(z)/\rho_X(0)$. $H_0 = H(z=0)$ is the Hubble constant. Ω_m and Ω_X are the ratios of the matter and dark energy density to the critical density $\rho_c^0 = 3H_0^2/(8\pi G)$, and $\Omega_k = -k/H_0^2$ with k denoting the curvature constant. Consistency of Eq.(2) at $z=0$ requires that $\Omega_m + \Omega_k + \Omega_X = 1$. Once $E(z)$ is specified, the evolution of matter density perturbations on large scales, $\delta^{(1)}(\mathbf{x}, t) = D_1(t)\delta(\mathbf{x})$ is determined by solving the following equation for $D_1 = \delta^{(1)}(\mathbf{x}, t)/\delta(\mathbf{x})$,

$$D_1''(\tau) + 2E(z)D_1'(\tau) - \frac{3}{2}\Omega_m(1+z)^3 D_1 = 0, \quad (3)$$

where primes denote $d/d(H_0 t)$. The linear growth rate

$$f_g(z) \equiv d \ln D_1 / d \ln a. \quad (4)$$

Note that we have assumed that dark energy and dark matter are separate, which is true for the vast majority of dark energy models that have been studied in the literature. If dark energy and dark matter are coupled (a more complicated possibility), or if dark energy and dark matter are unified (unified dark matter models), Eq.(3) would need to be modified accordingly. Ref.[20] found the first strong evidence for the separation of dark energy and dark matter by ruling out a broad class of so-called unified dark matter models. They showed that these models produce oscillations or exponential blowup of the dark matter power spectrum inconsistent with observation.

In the simplest alternatives to dark energy, the present cosmic acceleration is caused by a modification to general relativity. Ref.[21] contains examples of studies of observational signatures of modified gravity models. The only rigorously worked example is the DGP gravity model [10, 22], which can be described by a modified Friedmann equation¹:

$$H^2 - \frac{H}{r_0} = \frac{8\pi G \rho_m}{3}, \quad (5)$$

where $\rho_m(z) = \rho_m(0)(1+z)^3$. Solving the above equation gives

$$E(z) = \frac{1}{2} \left\{ \frac{1}{H_0 r_0} + \sqrt{\frac{1}{(H_0 r_0)^2} + 4\Omega_m^0(1+z)^3} \right\}, \quad (6)$$

with $\Omega_m^0 \equiv \rho_m(0)/\rho_c^0$, $\rho_c^0 \equiv 3H_0^2/(8\pi G)$. The added superscript “0” in Ω_m^0 denotes that this is the matter fraction today in the DGP gravity model. Note that consistency at $z=0$, $H(0) = H_0$ requires that $H_0 r_0 = 1/(1 - \Omega_m^0)$, so the DGP gravity model is parametrized by a single parameter, Ω_m^0 . The linear growth factor in the DGP gravity model is given by [22]

$$D_1''(\tau) + 2E(z)D_1'(\tau) - \frac{3}{2}\Omega_m(1+z)^3 D_1 \left(1 + \frac{1}{3\alpha_{DGP}} \right) = 0, \quad (7)$$

where $\alpha_{DGP} = [1 - 2H_0 r_0 + 2(H_0 r_0)^2]/(1 - 2H_0 r_0)$.

The dark energy model equivalent of the DGP gravity model is specified by requiring $8\pi G \rho_{de}^{eff}/3 = H/r_0$. Eq.(5) and the conservation of energy and momentum equation, $\dot{\rho}_{de}^{eff} + 3(\rho_{de}^{eff} + p_{de}^{eff})H = 0$, implies that $w_{de}^{eff} = -1/[1 + \Omega_m(a)]$ [22], where $\Omega_m(a) \equiv 8\pi G \rho_m(z)/(3H^2) = \Omega_m^0(1+z)^3/E^2(z)$. As $a \rightarrow 0$, $\Omega_m(a) \rightarrow 1$, and $w_{de}^{eff} \rightarrow -0.5$. As $a \rightarrow 1$, $\Omega_m(a) \rightarrow \Omega_m^0$, and $w_{de}^{eff} \rightarrow -1/(1 + \Omega_m^0)$. This means that the matter transfer function for the dark energy model equivalent of viable DGP

¹ The validity of the DGP model has been studied by [23].

gravity model ($\Omega_m^0 < 0.3$ and $w \leq -0.5$) are very close to that of the Λ CDM model at $k \gtrsim 0.001 h \text{ Mpc}^{-1}$. [24]

It is very easy and straightforward to integrate Eqs.(3) and (7) to obtain $D_1(a)$ for dark energy models and DGP gravity models, with the initial condition that for $a \rightarrow 0$, $D_1(a) = a$ (which assumes that the dark energy or modified gravity are negligible at sufficiently early times).

The measurement of $H(z)$ or $\rho_X(z)$ allows us to determine whether dark energy is a cosmological constant. The measurement of $f_g(z)$ allows us to determine whether gravity is modified.

III. OBSERVATIONAL METHODS

I will discuss the use of Type Ia supernovae, galaxy redshift surveys, weak lensing, and galaxy clusters in probing dark energy. These are recognized by the community as the most promising methods for dark energy search. Cosmic microwave background anisotropy (CMB) data and independent measurements of H_0 are required to break the degeneracy between dark energy and cosmological parameters (see e.g. [3]), hence are important as well in dark energy search.

A. Type Ia supernovae as dark energy probe

The use of Type Ia supernovae (SNe Ia) is the best established method for probing dark energy, since this is the method through which cosmic acceleration has been discovered [1, 2]. The unique advantage of this method is that it is independent of the clustering of matter, and can provide a robust measurement of $H(z)$ through the measured luminosity distance as a function of redshift, $d_L(z) = (1+z)r(z)$, where the comoving distance $r(z)$ from the observer to redshift z is given by

$$r(z) = cH_0^{-1} |\Omega_k|^{-1/2} \text{sinn}[\Omega_k^{1/2} \Gamma(z)], \quad (8)$$

$$\Gamma(z) = \int_0^z \frac{dz'}{E(z')}, \quad E(z) = H(z)/H_0$$

where $\text{sinn}(x) = \sin(x)$, x , $\sinh(x)$ for $\Omega_k < 0$, $\Omega_k = 0$, and $\Omega_k > 0$ respectively.

A SN Ia is a thermonuclear explosion that completely destroys a carbon/oxygen white dwarf at the Chandrasekhar limit of $1.4 M_\odot$.² This is the reason SNe Ia are so uniform in peak luminosity. The first challenge to overcome when using SNe Ia as cosmological standard candles is properly incorporating the intrinsic scatter in SN Ia peak luminosity. The usual calibration of SNe Ia reduces the intrinsic scatter in SN Ia peak luminosity (Hubble diagram dispersion) to about 0.16 mag [26, 27].

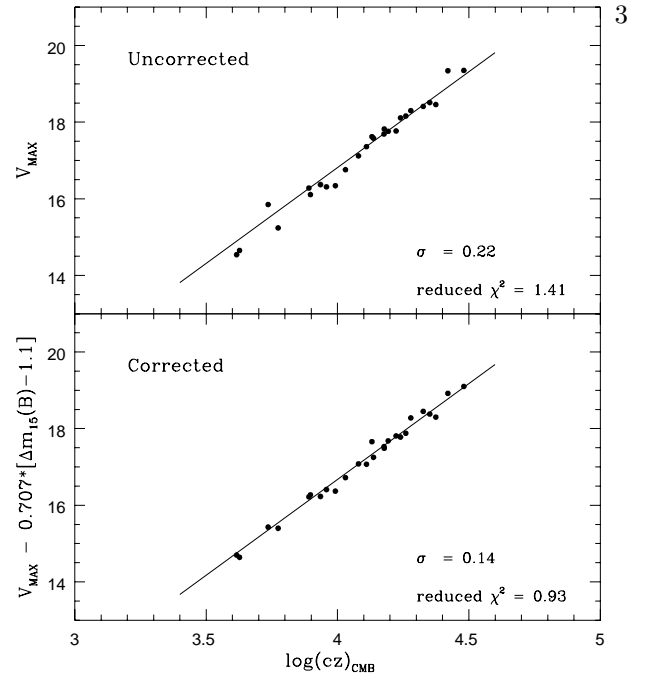


FIG. 3: Hubble diagrams showing 26 SNe Ia with $B_{max} - V_{max} \leq 0.20$ from the Calan/Tololo sample [32]. This sample provided half of the data for the discovery of the cosmic acceleration in 1998 [1]. The solid lines indicate Hubble's law; perfect standard candles (with $\sigma = 0$) fall on these lines.

The calibration techniques used so far are based on one observable parameter, the lightcurve width, which can be parametrized either as Δm_{15} (decline in magnitudes for a SN Ia in the first 15 days after B -band maximum, see [26]), or a stretch factor (which linearly scales the time axis, see [28]). The lightcurve width is associated with the amount of ^{56}Ni produced in the SN Ia explosion, which in turn depends on when the carbon burning makes the transition from turbulent deflagration to a supersonic detonation [29]. There may be additional physical parameters associated with SN Ia lightcurves [30] or spectra [31] that can further improve the calibration of SNe Ia. Fig.3 shows the homogeneity of SNe Ia [32]. Fig.4 shows the most recent homogeneous sample of SNe Ia [5].

The key to the efficient use of SNe Ia for probing dark energy is to obtain the largest possible unbiased sample of SNe Ia at the greatest distances from the observer [33]. This is achieved by an ultra deep survey of the same areas in the sky every few days over at least one year [34]. Fig.5 compared an ultra deep supernova survey [34] with a much shallower survey. Clearly, a sufficiently deep supernova survey is required to reconstruct the dark energy density $\rho_X(z)$ as a free function of cosmic time (i.e., to measure $H(z)$ precisely).

The main systematic effects for using SNe Ia to probe dark energy are: extinction by normal [35] or gray dust [36], weak lensing amplification by cosmic large scale structure [39], and possible evolution in the peak luminosity of SNe Ia.

Gray dust, consisting of large dust grains, is difficult

² The exception recently found by [25] is super-luminous and can be easily separated from the normal SNe Ia used for cosmology.

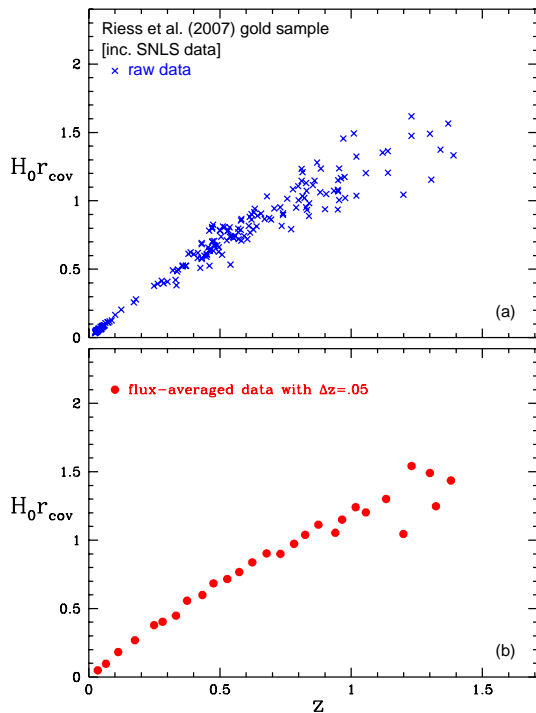


FIG. 4: The distance-redshift diagram of the most recent homogeneous sample of SNe Ia compiled by [5], including data from HST [5], SNLS [6], and nearby SNe Ia. This is an updated version of Fig.1 in [12]. Here $r_{cov} = r(z)$ is the comoving distance of an object at redshift z .

to detect by its reddening and could mimic the effect of dark energy [36]. Gray dust can be constrained quantitatively by the Cosmic Far Infrared Background [37], with no evidence found in favor of gray dust so far. Supernova flux correlation measurements can be used in combination with other lensing data to infer the level of dust extinction, and provide a viable method to eliminate possible gray dust contamination in SN Ia data [38].

The extinction by normal dust can be corrected using multi-band imaging data. Recent data show that the apparent dust extinction of SNe Ia is very different from the typical extinction law due to Milky Way dust, possibly due to the mixing of intrinsic SN Ia color variation with dust extinction, or variations in the properties of dust [40]. The key to minimizing the systematic effect due to dust extinction is to observe SNe Ia in the near infrared (NIR), since dust extinction decreases with wavelength.

NIR observations of SNe Ia have an important added advantage: SNe Ia are even better standard candles at NIR wavelengths [41, 42, 43]. Fig.6 shows the Hubble diagram of SNe Ia in the NIR, *without* the usual lightcurve width correction.

The weak lensing amplification of SNe Ia by cosmic large scale structure can be modeled by a universal probability distribution function for weak-lensing amplification based on the measured matter power spectrum [44]. The effect of weak lensing on the SN Ia data can be minimized through flux-averaging [45].

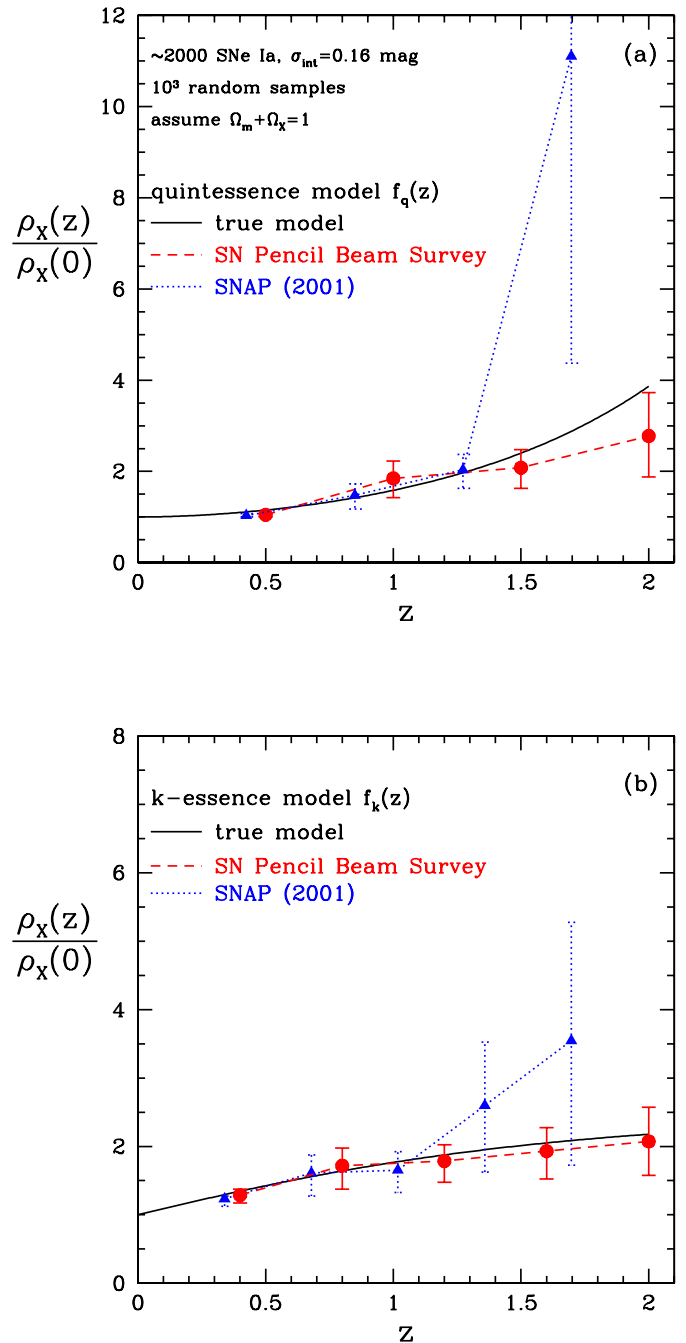


FIG. 5: The comparison of an ultra deep supernova survey [34] with a much shallower survey in the reconstruction of the dark energy density $\rho_X(z)$ as a free function of cosmic time [33].

The evolution in SN Ia peak luminosity could arise due to progenitor population drift, since the most distant SNe Ia come from a stellar environment very different (a much younger universe) than that of the nearby SNe Ia. However, with sufficient statistics, we can subtype SNe Ia and compare SNe Ia at high redshift and low redshift that are

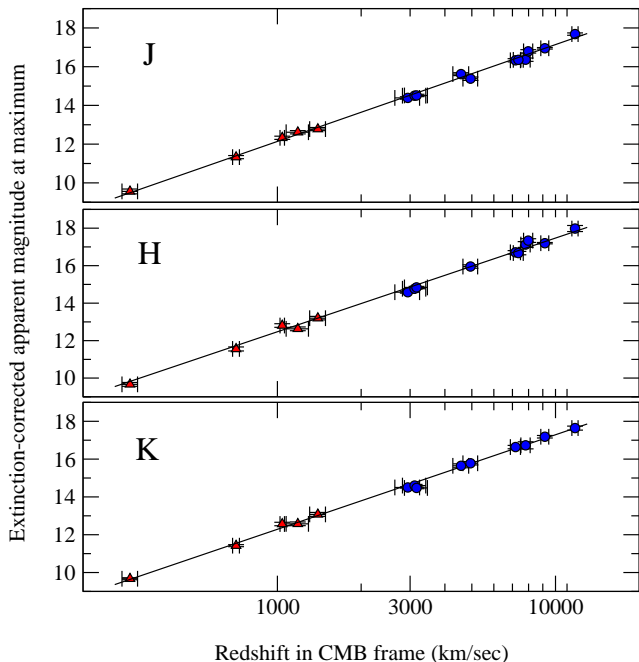


FIG. 6: Hubble diagrams of SNe Ia in the NIR bands. Note that these SNe Ia have only been corrected for dust extinction; *no* corrections have been made for lightcurve width. [41]

similar in both lightcurves and spectra, thus overcoming the possible systematic effect due to progenitor population drift [46].

B. Galaxy redshift survey as dark energy probe

A magnitude-limited galaxy redshift survey can allow us to measure the cosmic expansion history $H(z)$ through baryon acoustic oscillations (BAO) in the galaxy distribution, and the growth history of cosmic large scale structure $f_g(z)$ through independent measurements of redshift-space distortions and the bias factor between the distribution of galaxies and that of matter.[51]

The use of BAO as a cosmological standard ruler is a relatively new method for probing dark energy [47, 48, 49], but it has already yielded impressive constraints on dark energy [7].

At the last scattering of CMB photons, the acoustic oscillations in the photon-baryon fluid became frozen, and imprinted their signatures on both the CMB (the acoustic peaks in the CMB angular power spectrum) and the matter distribution (the baryon acoustic oscillations in the galaxy power spectrum). Because baryons comprise only a small fraction of matter, and the matter power spectrum has evolved significantly since last scattering of photons, BAO are much smaller in amplitude than the CMB acoustic peaks, and are washed out on small scales.

BAO in the observed galaxy power spectrum have the characteristic scale determined by the comoving sound horizon at recombination, which is precisely measured

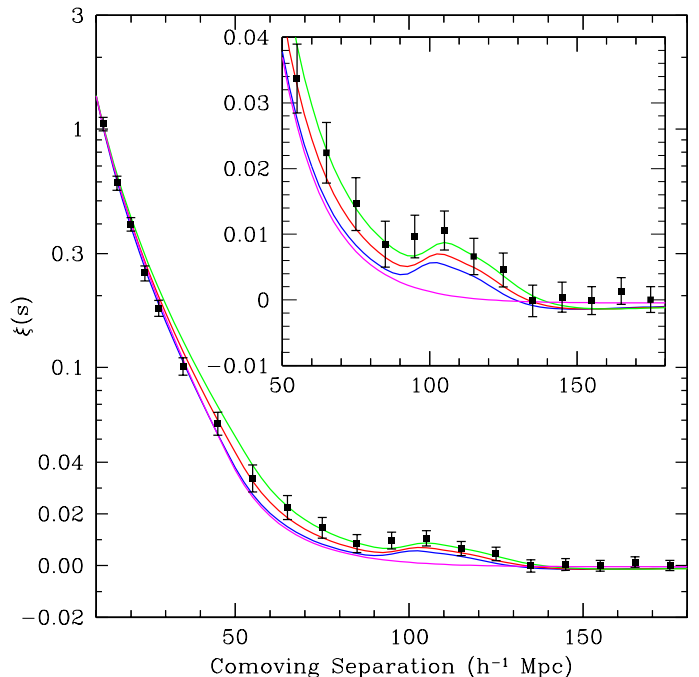


FIG. 7: The galaxy correlation function measured from the SDSS data, clearly showing a peak corresponding to the BAO scale at $\sim 100 h^{-1} \text{Mpc}$ [7].

by the CMB anisotropy data [4]. Comparing the observed BAO scales with the expected values gives $H(z)$ in the radial direction, and $D_A(z) = r(z)/(1+z)$ (the angular diameter distance) in the transverse direction. Fig.7 shows the BAO scale measurement by the SDSS team, which is usually quoted in the form of $A_{BAO} = 0.469 (n_S/0.98)^{-0.35} \pm 0.017$ (with n_S denoting the power-law index of the primordial matter power spectrum), to be compared with the theoretical prediction of

$$A = \left[r^2(z_{BAO}) \frac{cz_{BAO}}{H(z_{BAO})} \right]^{1/3} \frac{(\Omega_m H_0^2)^{1/2}}{cz_{BAO}}, \quad (9)$$

with $z_{BAO} = 0.35$. [7]

A magnitude-limited galaxy redshift survey can allow us to measure both $H(z)$ and $f_g(z)$ [50, 51]. The measurement of $f_g(z)$ can be obtained through independent measurements of redshift-space distortion parameter $\beta = f_g(z)/b$ [52] and the bias parameter $b(z)$ (which describes how light traces mass) [50]. The parameter β can be measured directly from galaxy redshift survey data by studying the observed redshift-space correlation function [53, 54]. We can assume that the galaxy density perturbation δ_g is related to the matter density perturbation $\delta(\mathbf{x})$ as follows [55]:

$$\delta_g = b\delta(\mathbf{x}) + b_2\delta^2(\mathbf{x})/2. \quad (10)$$

The galaxy bispectrum is

$$\langle \delta_{g\mathbf{k}_1} \delta_{g\mathbf{k}_2} \delta_{g\mathbf{k}_1} \rangle = (2\pi)^3 \{ P_g(\mathbf{k}_1) P_g(\mathbf{k}_2) [J(\mathbf{k}_1, \mathbf{k}_2)/b + b_2/b^2] + c_{yc}. \} \delta^D(\mathbf{k}_1 + \mathbf{k}_2 + \mathbf{k}_3), \quad (11)$$

where J is a function that depends on the shape of the triangle formed by $(\mathbf{k}_1, \mathbf{k}_2, \mathbf{k}_3)$ in \mathbf{k} space, but only depends very weakly on cosmology [56]. Ref.[56] developed the method for measuring $b(z)$ from the galaxy bispectrum, which was applied by [57] to the 2dF data. Independent measurements of $\beta(z)$ and $b(z)$ have only been published for the 2dF data [53, 57].

Fig.8 shows how well a magnitude-limited NIR galaxy redshift survey covering $>10,000$ square degrees and $0.5 < z < 2$ can constrain $H(z)$ and $f_g(z)$, compared with current data [51]. Fig.8(b) shows the $f_g(z)$ for a modified gravity model (the DGP gravity model) with $\Omega_m^0 = 0.25$ (solid line), as well as a dark energy model that gives the same $H(z)$ for the same Ω_m^0 (dashed line). The cosmological constant model from Fig.8(a) is also shown (dotted line). Clearly, current data can not differentiate between dark energy and modified gravity. A very wide and deep galaxy redshift survey provides measurement of $f_g(z)$ accurate to a few percent [see Fig.8(b)]; this will allow an unambiguous distinction between dark energy models and modified gravity models that give identical $H(z)$ [see the solid and dashed lines in Fig.8(b)]. For a linear cutoff given by $\sigma^2(R) = 0.35$ (or 0.2), a survey covering $11,931 (\text{deg})^2$ would rule out the DGP gravity model that gives the same $H(z)$ and Ω_m^0 at 99.99% (or 95%) C.L.; a survey covering $13,912 (\text{deg})^2$ would rule out the DGP gravity model at 99.999% (or 99%) C.L. [51].

The systematic effects of BAO as a standard ruler are: bias between luminous matter and matter distributions, nonlinear effects, and redshift distortions [47, 48]. Cosmological N-body simulations are required to quantify these effects [58, 59, 60, 61]. Ref.[62] shows that nonlinear effects can be accurately taken into account. Ref.[63] shows that the BAO signal is *boosted* when bias, nonlinear effects, and redshift distortions are properly included in the Hubble Volume simulation.

C. Weak lensing as dark energy probe

Weak lensing usually refers to the statistically correlated image distortions of background galaxies due to the foreground matter distribution, also known as “cosmic shear”. The first conclusive detection of cosmic shear was made in 2000 [64].

Fig.9 shows the constraints on cosmological parameters σ_8 (the amplitude of matter density fluctuations averaged on the scale of $8 h^{-1} \text{Mpc}$), Ω_m , and a constant dark energy equation of state $w = w_0$ from current weak lensing data [65]. Fig.10 shows how the measurement of σ_8 has evolved over the last several years [66].

Fig.9 and Fig.10 illustrate both the advantage and the disadvantage of weak lensing as dark energy probe. weak lensing has the advantage of being sensitive to the clustering of matter, which can potentially allow us to differentiate between dark energy and modified gravity [69]. However, if the clustering of matter is not accurately measured, the uncertainty is propagated into the mea-

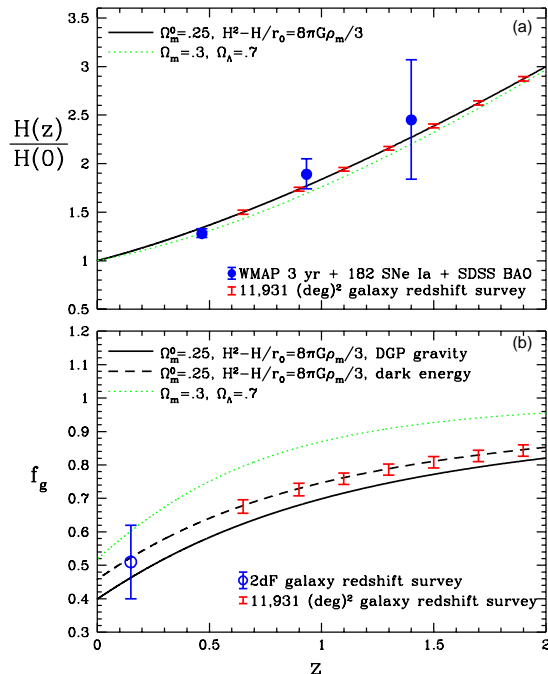


FIG. 8: Current and expected future measurements of the cosmic expansion history $H(z) = H_0 E(z)$ and the growth rate of cosmic large scale structure $f_g(z) = d \ln \delta / d \ln a$ ($\delta = (\rho_m - \overline{\rho_m}) / \overline{\rho_m}$, a is the cosmic scale factor). The future data correspond to a magnitude-limited NIR galaxy redshift survey covering $>10,000$ square degrees and $0.5 < z < 2$. If the $H(z)$ data are fit by both a DGP gravity model and an equivalent dark energy model that predict the same expansion history, a survey area of $11,931 (\text{deg})^2$ is required to rule out the DGP gravity model at the 99.99% confidence level. [51]

surement of dark energy parameters (see Fig.9).

If the systematic effects are properly modeled, a weak lensing survey can potentially allow us to differentiate between dark energy and modified gravity (see Fig.11) [69]. Fig.11 assumed a “ 2π ” deep and wide survey of 20,000 square degrees in six wavelength bands from $0.4 - 1.1 \mu\text{m}$ to be undertaken by the Large Synoptic Survey Telescope (LSST). This survey will yield the shear and photometric redshift of 3 billion source galaxies over a redshift range of 0.2 to 3. [69]

Weak lensing can be used to probe dark energy in two different ways: weak lensing tomography [64], or weak lensing cross-correlation cosmography [67] (also known as “the geometric method” [68]). Much of the effort has been focused on using the geometric weak lensing method to probe dark energy to minimize the sensitivity to the clustering of matter (which can be a source of systematic uncertainty).

The basic idea of the geometric weak lensing method is to construct a map of the foreground galaxies, from which an estimated map of the foreground mass can be made. This foreground mass slice induces shear on all the galaxies in the background. The amplitude of the induced shear as a function of the background redshift

is measured, from which a weighted sum of the ratios of angular diameter distances between the source slice and lens slice, and between the lens slice and observer is estimated. [67, 68] Note that this marks an important difference of the weak lensing method from the supernova and baryon acoustic oscillation methods: the weak lensing method gives correlated measurements of the cosmic expansion history $H(z)$ in redshift bins, while the supernova and baryon acoustic oscillation methods can give uncorrelated measurements of $H(z)$ [12, 48].

In the geometric weak lensing method, photometric redshifts³ are used to divide galaxies into redshift bins. The centroids of the photometric redshifts must be known to the accuracy of around 0.1% in order to avoid significant degradation of dark energy constraints [70, 71] (see Fig.12).

In addition to the uncertainty in the centroids of photometric redshift bins, there are other systematic uncertainties in the use of weak lensing as dark energy probe. These include point spread function (PSF) correction, bias in the selection of the galaxy sample, and the intrinsic distortion signal due to the intrinsic alignment of galaxies (see the detailed discussion in Ref.[72]).

D. Clusters as dark energy probe

Clusters of galaxies can be used to probe dark energy in two different ways: (1) using the cluster number density and its redshift evolution, as well as cluster distribution on large scales (see for example [73, 74, 75]); (2) using clusters as standard candles by assuming a constant cluster baryon fraction (see for example, [76]), or using combined X-ray and SZ measurements for absolute distance measurements (see for example [77]).

Large, well-defined and statistically complete samples of galaxy clusters are required to derive robust dark energy constraints from cluster data. Future surveys aim to select clusters using data from X-ray satellite with high resolution and wide sky coverage, and multi-band optical and near-IR surveys to obtain photometric redshifts for clusters.[73]

The systematic uncertainties of clusters as dark energy probe include uncertainty in the cluster mass estimates that are derived from observed properties, such as X-ray or optical luminosities and temperature (e.g. [78, 79, 80]). Fig.13 shows the total cluster mass versus a proxy based on the total baryon mass and temperature (both of which can be inferred from X-ray observations), based on simulated X-ray data [81].

IV. CURRENT STATUS AND FUTURE PROSPECTS

There are a large number of dark energy surveys that are ongoing or have been proposed. Ongoing projects include *Essence* [82], *Supernova Legacy Survey (SNLS)* [83], *Carnegie Supernova Project (CSP)* [84], *ESO Visible and Infrared Survey Telescope for Astronomy (VISTA) Surveys* [85], *Panoramic Survey Telescope & Rapid Response System (Pan-STARRS)* [86], and *WiggleZ* [87]. Proposed near term projects include *Advanced Liquid-mirror Probe for Astrophysics, Cosmology and Asteroids (ALPACA)* [88]; *Dark Energy Survey (DES)* [89]; *Hobby-Eberly Telescope Dark Energy Experiment (HETDEX)* [90]; *Wide-Field Multi-Object Spectrograph* [91] and *Sloan Digital Sky Survey (SDSS) III* [92]. Proposed long-term projects include *Large Synoptic Survey Telescope (LSST)* [94], *Joint Dark Energy Mission (JDEM)* [93], *Square Kilometre Array (SKA)* [95], and an European-led dark energy mission [96].

The U.S. Dark Energy Task Force (DETF) has recommended an aggressive, multi-stage, multi-method program to explore dark energy as fully as possible.[97] DETF recommended a dark energy program with multiple techniques at every stage, with at least one of these being a probe sensitive to the growth of cosmic structure in the form of galaxies and clusters of galaxies.

The DETF defined a figure of merit that is the inverse of the area of the 95% confidence level error ellipse in the w_0-w_a plane [assuming a dark energy equation of state $w_X(a) = w_0 + w_a(1 - a)$]. DETF recommended that dark energy program in Stage III (near-term, medium-cost projects) should be designed to achieve at least a factor of 3 gain over Stage II (ongoing projects) in the figure of merit, and that dark energy program in Stage IV (long-term, high-cost projects JDEM, LST, SKA) should be designed to achieve at least a factor of 10 gain over Stage II in the figure of merit.

The DETF recommended continued research and development investment to optimize JDEM, LST, and SKA (Stage IV) to address remaining technical questions and systematic-error risks, and high priority for near-term projects to improve understanding of dominant systematic effects in dark energy measurements, and wherever possible, reduce them. The DETF recommended a coherent program of experiments designed to meet the goals and criteria it proposed.

The ESA-ESO Working Group on Fundamental Cosmology made specific recommendations to ESA and ESO. It recommended a wide-field optical and near-IR imaging survey (suitable for weak lensing and cluster surveys) as a high priority, with ESA launching a satellite for high resolution wide-field optical and near-IR imaging, and ESO carrying out optical multi-color photometry, as well as a large spectroscopic survey (>100,000 redshifts over ~10,000 square degrees) to calibrate photometric redshifts. They also recommended that ESA-ESO secure access to an instrument with capability for massive mul-

³ Photometric redshifts are approximate redshifts estimated from multi-band imaging data. They are calibrated using a spectroscopic sample.

tiplexed deep spectroscopy (several thousand simultaneous spectra over one square degree) (suitable for large galaxy redshift surveys), as well as conduct a supernova survey with multi-color imaging to extend existing samples of $z = 0.5 - 1$ SNe by an order of magnitude, and improve the local sample of SNe. They suggested the use of a European Extremely Large Telescope (ELT) to study SNe at $z > 1$.

The U.S. National Research Council's Committee on NASA's Beyond Einstein Program recently made the recommendation that NASA and DOE should proceed immediately with a competition to select a JDEM for a 2009 new start. They concluded that "The broad mission goals in the Request for Proposal should be (1) to determine the properties of dark energy with high precision and (2) to enable a broad range of astronomical investigations. The committee encourages the Agencies to seek as wide a variety of mission concepts and partnerships as possible."

ESA's Cosmic Vision 2015-2025 recently made the first selection of candidate missions for assessment studies. These include two mission concept for a European-led

dark energy mission: DUNE, the Dark UNiverse Explorer [98], and SPACE, the SPectroscopic All-sky Cosmic Explorer [99]. The synergy between JDEM and the ESA-led dark energy mission will be important for a strategically optimized approach to discovering the nature of dark energy.

In evaluating the various dark energy projects, it is critical to note that the challenge to solving the dark energy mystery will not be the statistics of the data obtained, but the tight control of systematic effects inherent in the data. A combination of the most promising methods (as discussed in this review), each optimized by having its systematics minimized by design, provides the tightest control of systematics [100]. The discovery of the nature of dark energy will revolutionize our understanding of the universe.

Acknowledgements: I am grateful to Daniel Eisenstein, Mario Hamuy, Marco Hettterscheidt, Henk Hoekstra, Dragan Huterer, Lloyd Knox, Andrey Kravtsov, and Kevin Krisciunas for permission to use their figures in this review paper.

-
- [1] A. G. Riess *et al.*, *Astron. J.*, **116**, 1009 (1998)
- [2] S. Perlmutter *et al.*, *ApJ*, **517**, 565 (1999)
- [3] Y. Wang, and P. Mukherjee P, astro-ph/0703780, PRD, in press (2007)
- [4] D. N. Spergel *et al.*, *ApJS*, **170**, 377 (2007)
- [5] A. G. Riess *et al.*, *ApJ* **659**, 98 (2007).
- [6] P. Astier *et al.*, *Astron. Astrophys.* **447**, 31 (2006);
- [7] D. Eisenstein *et al.*, *ApJ* **633**, 560 (2005);
- [8] K. Freese *et al.*, *Nucl.Phys.* **B287**, 797 (1987); A. Linde, in *Three hundred years of gravitation*, (Eds.: Hawking, S.W. and Israel, W., Cambridge Univ. Press, 1987), 604; P. J. E Peebles and B. Ratra, *ApJ* **325**, L17 (1988); C. Wetterich, *Nucl.Phys.* **B302**, 668 (1988); J. A. Frieman, C. T. Hill, A. Stebbin, and I. Waga, *PRL* **75**, 2077 (1995); R. Caldwell, R. Dave, and P. J. Steinhardt, *PRL* **80**, 1582 (1998); L. Wang and P. J. Steinhardt, *ApJ* **508**, 483 (1998).
- [9] V. Sahni and S. Habib, *PRL* **81**, 1766 (1998); L. Parker and A. Raval, *PRD* **60**, 063512 (1999); C. Deffayet, *Phys.Lett.B* **502**, 199 (2001); K. Freese and M. Lewis, *Phys.Lett.B* **540**, 1 (2002); V. K. Onemli and R. P. Woodard, *PRD* **70**, 107301 (2004).
- [10] G. Dvali, G. Gabadadze, M. Porrati, *PLB*, **485**, 208 (2000)
- [11] T. Padmanabhan, *Phys.Rep.* **380**, 235 (2003); P. J. E Peebles and B. Ratra, *Rev.Mod.Phys.* **75**, 55 (2003); V. Sahni and A. Starobinsky, *IJMPD* **15**, 2105 (2006); E. J. Copeland, M. Sami, and S. Tsujikawa, *IJMPD* **15**, 1753 (2006); P. Ruiz-Lapuente, *Class. Quantum Grav.* **24**, R91 (2007); B. Ratra and M. S. Vogeley, arXiv:0706.1565 (2007).
- [12] Y. Wang, & M. Tegmark, *Phys. Rev. D* **71**, 103513 (2005)
- [13] J. Simon, L. Verde, & R. Jimenez, R., *PRD*, **71**, 123001 (2005); V. Barger, Y. Gao, D. Marfatia, astro-ph/0611775; H.K. Jassal, J.S. Bagla, T. Padmanabhan, astro-ph/0601389; J. Dick, L. Knox, M. Chu, *JCAP* **0607**, 001 (2006); C. Li, D.E. Holz, & A. Cooray, astro-ph/0611093; A.R. Liddle; P. Mukherjee, D. Parkinson, Y. Wang, *PRD*, **74**, 123506 (2006); S. Nesseris, & L. Perivolaropoulos, astro-ph/0612653; K.M. Wilson, G. Chen, B. Ratra, astro-ph/0602321; J.-Q. Xia, et al., *PRD*, **74**, 083521 (2006); U. Alam, V. Sahni, A.A. Starobinsky, *JCAP*, **0702**, 011 (2007); R. A. Daly, et al., arXiv:0710.5112; R. Caldwell, A. Cooray, A. Melchiorri, astro-ph/0703375
- [14] Chevallier, M., & Polarski, D. 2001, *Int. J. Mod. Phys. D10*, 213
- [15] Y. Wang, and P. Garnavich, *ApJ*, **552**, 445 (2001)
- [16] M. Tegmark, *Phys. Rev. D* **66**, 103507 (2002)
- [17] Y. Wang, & K. Freese, *Phys.Lett. B* **632**, 449 (2006); astro-ph/0402208
- [18] Y. Wang; J.M. Kratochvil; A. Linde; M. Shmakova, *JCAP*, **12**, 006 (2004)
- [19] Y. Wang, & M. Tegmark, *Phys. Rev. Lett.*, **92**, 241302 (2004)
- [20] H.B. Sandvik; M. Tegmark; M. Zaldarriaga; I. Waga, *Phys. Rev. D* **69**, 123524 (2004)
- [21] J-P. Uzan, and F. Bernardeau, *Phys. Rev. D* **64**, 083004 (2001); H. F. Stabenau and B. Jain, *PRD*, **74**, 084007; (2006) A. F. Heavens, T.D. Kitching, L. Verde, astro-ph/0703191; J.-P. Uzan, *Gen. Relat. Grav.* **39**, 307 (2007) P. Zhang; M. Liguori; R. Bean; S. Dodelson, *Phys.Rev.Lett.* **99**, 141302 (2007)
- [22] A. Lue, R. Scoccimarro, and G. D. Starkman, *PRD* **69**, 124015 (2004); A. Lue, *Physics Report* **423**, 1 (2006).
- [23] Y.-S. Song, I. Sawicki, and W. Hu, *PRD*, **75**, 064003 (2007); K. Koyama, arXiv:0709.2399
- [24] C. P. Ma, R. R. Caldwell, P. Bode, and L. Wang, *ApJ*,

- 521**, L1 (1999)
- [25] D. A. Howell, et al., *Nature* **443**, 308 (2006)
- [26] M. M. Phillips, *ApJ* **413**, L105 (1993);
- [27] A.G. Riess, W.H. Press, & R.P. Kirshner, *ApJ*, **438**, L17 (1995)
- [28] G. Goldhaber, et al, *ApJ*, **558**, 359 (2001)
- [29] Wheeler, J. C., AAPT/AJP Resource Letter, *Am. J. Phys.*, **71** (2003), astro-ph/0209514
- [30] Y. Wang, and N. Hall, *MNRAS*, submitted (2007), arXiv:0711.1560 [astro-ph]
- [31] See for example, S. Bongard, et al., *ApJ*, **647**, 513 (2006); D. Branch, et al., *PASP*, **118**, 560 (2006)
- [32] M. Hamuy, et al., *AJ*, **112**, 2398 (1996)
- [33] Y. Wang, & G. Lovelace, *ApJ Letter*, **562**, L115 (2001)
- [34] Y. Wang, *ApJ*, **531**, 676 (2000), astro-ph/9806185
- [35] J.A. Cardelli; G.C. Clayton; & J.S. Mathis, *ApJ*, **345**, 245 (1989)
- [36] A.N. Aguirre, *ApJ*, **525**, 583 (1999)
- [37] A.N. Aguirre, and Z. Haiman, *ApJ*, **532**, 28 (2000)
- [38] P. Zhang, and P.S. Corasanti, *ApJ*, **657**, 71 (2007)
- [39] R. Kantowski, T. Vaughan, & D. Branch, *ApJ*, **447**, 35 (1995); J. A. Frieman, *Comments Astrophys.*, **18**, 323 (1997); J. Wambsganss, R. Cen, G. Xu, & J.P. Ostriker, *ApJ*, **475**, L81 (1997); D.E. Holz, *ApJ*, **506**, L1 (1998); Y. Wang, *ApJ*, **525**, 651 (1999)
- [40] Conley, A., et al. 2007, arXiv:0705.0367v2, *ApJL*, in press
- [41] K. Krisciunas; M.M. Phillips; N.B. Suntzeff, *ApJ*, **602**, L81 (2004)
- [42] M. M. Phillips; P. Garnavich; Y. Wang; et al., astro-ph/0606691, published in SPIE proceedings (2006)
- [43] W. Michael Wood-Vasey, et al., arXiv:0711.2068, *ApJ* submitted (2007)
- [44] Y. Wang; D.E. Holz; & D. Munshi, *ApJ*, **572**, L15 (2002)
- [45] Y. Wang, *ApJ*, **536**, 531 (2000); Y. Wang; & P. Mukherjee, *ApJ*, **606**, 654 (2004).
- [46] D. Branch; S. Perlmutter; E. Baron; & P. Nugent, astro-ph/0109070 (2001), Contribution to the SNAP (Supernova Acceleration Probe) Yellow Book (Snowmass 2001)
- [47] C. Blake and K. Glazebrook, *ApJ*, **594**, 665 (2003)
- [48] H. Seo and D. J. Eisenstein, *ApJ*, **598**, 720 (2003)
- [49] See for example, M. White, *Astropart. Phys.* **24**, 334 (2005); G. Huetsi, *A&A* **449**, 891 (2006); Y. Wang, *ApJ* **647**, 1 (2006); R. Angulo *et al.*, astro-ph/0702543. (2007). See <http://cdm.berkeley.edu/doku.php?id=baopages> for a more complete list of references.
- [50] Guzzo L *et al.*, *Nature*, in press (2008)
- [51] Y. Wang, arXiv:0710.3885v1 [astro-ph]
- [52] N. Kaiser, *MNRAS*, **227**, 1 (1987)
- [53] E. Hawkins *et al.*, *MNRAS*, **346**, 78 (2003)
- [54] M. Tegmark *et al.*, *PRD* **74**, 123507 (2006); N. P. Ross *et al.*, *MNRAS* **381**, 573 (2007); J. da Angela *et al.*, astro-ph/0612401.
- [55] J. N. Fry and E. Gaztanaga, *ApJ*, **413**, 447 (1993)
- [56] S. Matarrese, L. Verde, and A. F. Heavens, *MNRAS*, **290**, 651 (1997)
- [57] L. Verde *et al.*, *MNRAS*, **335**, 432 (2002)
- [58] Angulo, R., et al. 2005, *Mon.Not.Roy.Astron.Soc.Lett.*, **362**, L25-L29
- [59] H. Seo and D. J. Eisenstein, *ApJ*, **633**, 575 (2005)
- [60] V. Springel, et al., *Nature*, **435**, 629 (2005)
- [61] White, M. 2005, *Astropart.Phys.* **24**, 334
- [62] D. Jeong and E. Komatsu, *ApJ* **651**, 619 (2006); M. Crocce, and R. Scoccimarro, arXiv:0704.2783; R. E. Smith, R. Scoccimarro, and R. K. Sheth, astro-ph/0703620;
- [63] R. S. Koehler, P. Schuecker, and K. Gebhardt, *A&A*, **462**, 7 (2007)
- [64] D. M. Wittman; J. A. Tyson; D. Kirkmand; I. Dell'Antonio; G. Bernstein, *Nature*, **405**, 143 (2000)
- [65] H. Hoekstra, et al., *ApJ*, **647**, 116 (2006)
- [66] M. Hettterscheidt, et al., *A&A*, **468**, 859 (2007)
- [67] B. Jain, & A. Taylor, *PRL*, **91**, 141302 (2003)
- [68] J. Zhang; L. Huim; A. Stebbins, *ApJ*, **635**, 806 (2005)
- [69] L. Knox, Y. S. Song, , and J. A. Tyson, *PRD*, **74**, 023512 (2006)
- [70] G. Bernstein, and B. Jain, *ApJ*, **600**, 17 (2004)
- [71] D. Huterer, et al., *MNRAS*, **366**, 101 (2006)
- [72] Peacock, J.A.; Schneider,P.; Efstathiou, G.; Ellis, J.R.; Leibundgut, B.; Lilly, S.J.; Mellier, Y. 2006, *Report by the ESA-ESO Working Group on Fundamental Cosmology*, arXiv:astro-ph/0610906
- [73] Z. Haiman; J.J. Mohr; G.P. Holder, *ApJ*, **553**, 545 (2001)
- [74] A. Vikhlinin, et al., *ApJ*, **590**, 15 (2003)
- [75] P. Schuecker, et al., *A&A*, **398**, 867 (2003)
- [76] S.W. Allen, et al., *MNRAS*, **353**, 457 (2004)
- [77] S.M. Molnar, et al., *ApJ*, **601**, 22 (2004)
- [78] S. Majumdar, & J.J. Mohr, *ApJ*, **585**, 603 (2003)
- [79] S. Majumdar, & J.J. Mohr, *ApJ*, **613**, 41 (2004)
- [80] M. Lima, & W. Hu, *PRD*, **70**, 043504 (2004)
- [81] A.V. Kravtsov, A. Vikhlinin, & D. Nagai, *ApJ*, **650**, 128 (2006)
- [82] <http://www.ctio.noao.edu/~wsne/>
- [83] <http://www.cfht.hawaii.edu/SNLS/>
- [84] <http://www.ociw.edu/csp/>
- [85] <http://www.vista.ac.uk/index.html>
- [86] <http://pan-starrs.ifa.hawaii.edu/public/>
- [87] <http://wigglez.swin.edu.au/Welcome.html>
- [88] <http://www.astro.ubc.ca/LMT/alpaca/index.html>
- [89] <http://www.darkenergysurvey.org/>
- [90] <http://www.as.utexas.edu/hetdex/>
- [91] <http://www.so.stfc.ac.uk/roadmap/rmProject.aspx?q=128>
- [92] <http://www.sdss.org/>
- [93] <http://universe.nasa.gov/program/probes/jdem.html>
- [94] <http://www.lsst.org/>
- [95] <http://www.skatelescope.org/>
- [96] <http://sci.esa.int/science-e/www/object/index.cfm?fobjectid=41438>
- [97] Albrecht, A.; Bernstein, B.; Cahn, R.; Freedman, W.L.; Hewitt, J.; Hu, W.; Huth, J.; Kamionkowski, M.; Kolb, E.W.; Knox, L.; Mather, J.C.; Staggs, S.; Suntzeff, N. B., *Report of the Dark Energy Task Force*, astro-ph/0609591
- [98] A. Refregier, et al., astro-ph/0610062; <http://www.dune-mission.net/>
- [99] M. Robberto, A. Cimatti, for the SPACE Science Team, arXiv:0710.3970; <http://urania.bo.astro.it/cimatti/space/>
- [100] Y. Wang *et al.*, *BAAS* **v36**, n5;1560 (2004); A. Crotts *et al.*, astro-ph/0507043 (2005); E. Cheng and Y. Wang *et al.*, *Proc. of SPIE* **Vol. 6265**, 626529 (2006).

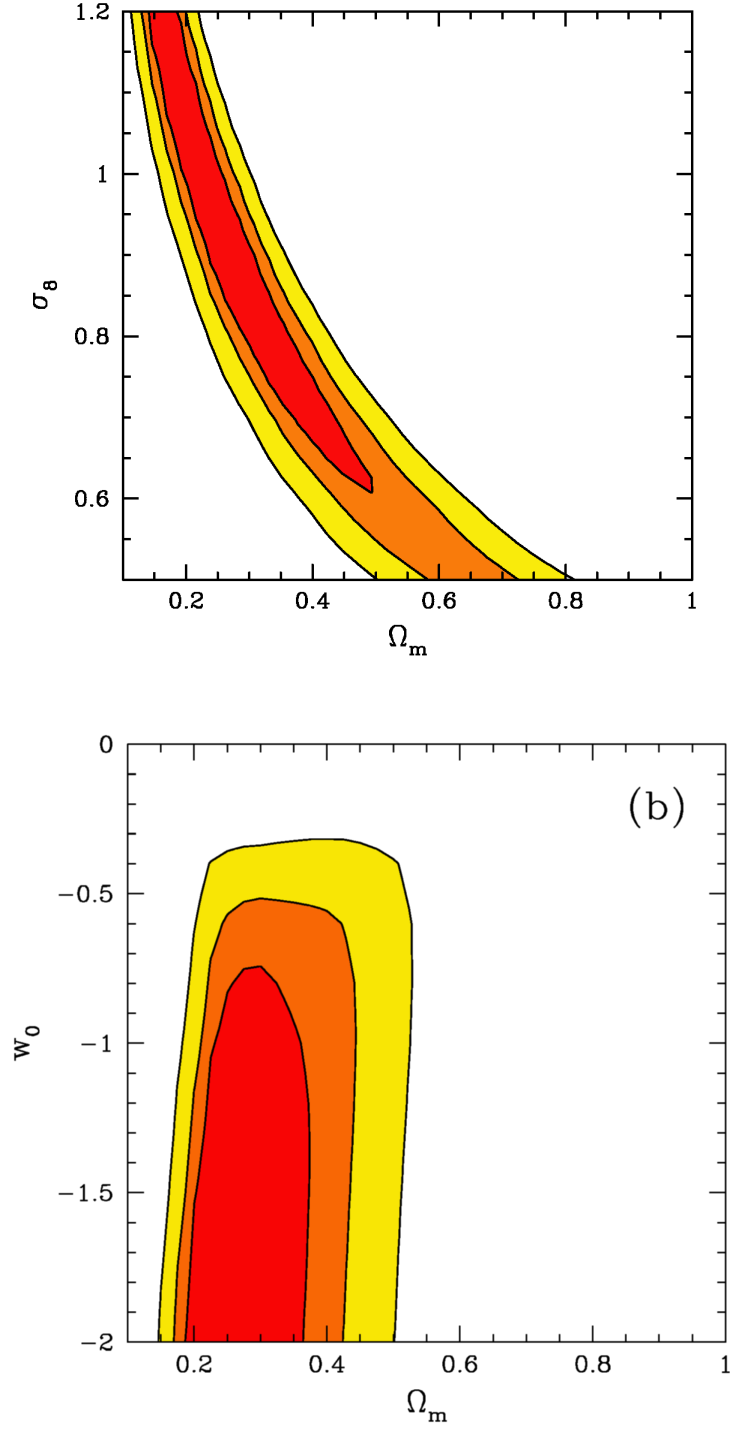


FIG. 9: Current constraints on cosmological parameters and dark energy from the CFHTLS Deep and Wide weak lensing survey, assuming a constant $w_X(z)$ and a flat universe. [65].

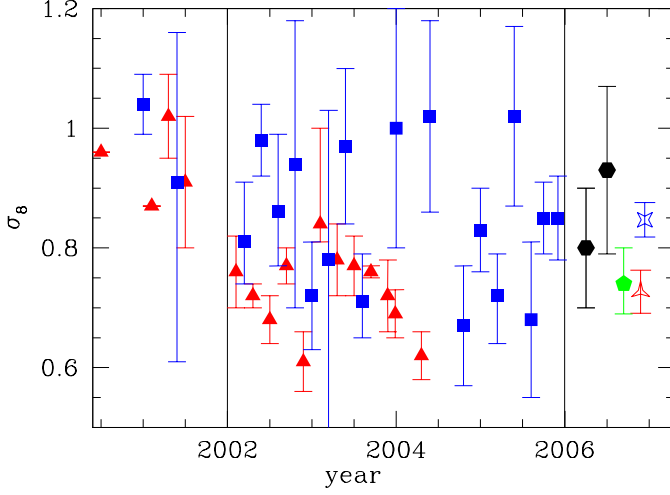


FIG. 10: The measurements of σ_8 from the analysis of clusters of galaxies (red) and cosmological weak lensing over the last several years. [66]

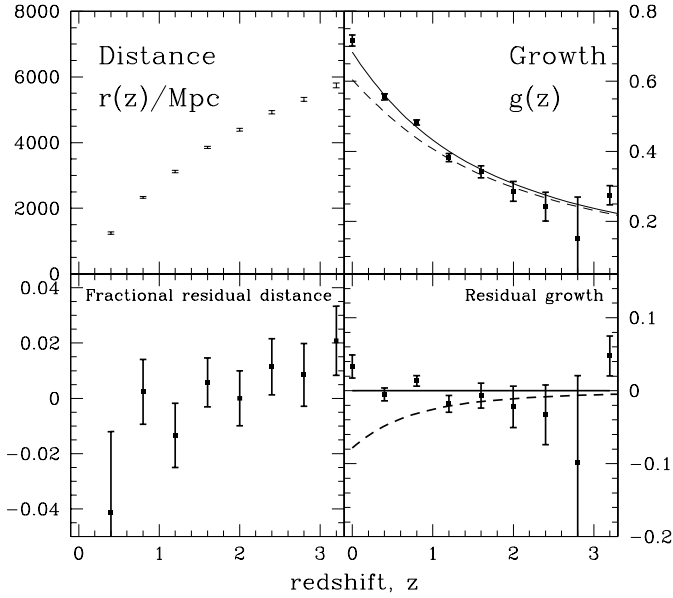


FIG. 11: Reconstructed distances (left panels), and growth factors (right panels) from a LSST-like weak lensing survey. The lower left panel shows the fractional residual distances, $[r(z) - r_{\text{fid}}(z)]/r_{\text{fid}}(z)$, where $r(z)$ are the reconstructed distances and $r_{\text{fid}}(z)$ are the distances in the fiducial DGP model. The lower right panel shows the residual growth factor, $g(z) - g_{\text{fid}}(z)$. The curves in the right panels are $g_{\text{fid}}(z)$ (solid) and $g(z)$ for the Einstein gravity model (dashed) with the same $H(z)$ and ρ_m as the DGP model. Although these two models have the same $r(z)$ they are distinguishable by their significantly different growth factors. [69]. Note that $g(z) \propto D_1(t)$ [see Eqs.(3) and (7)].

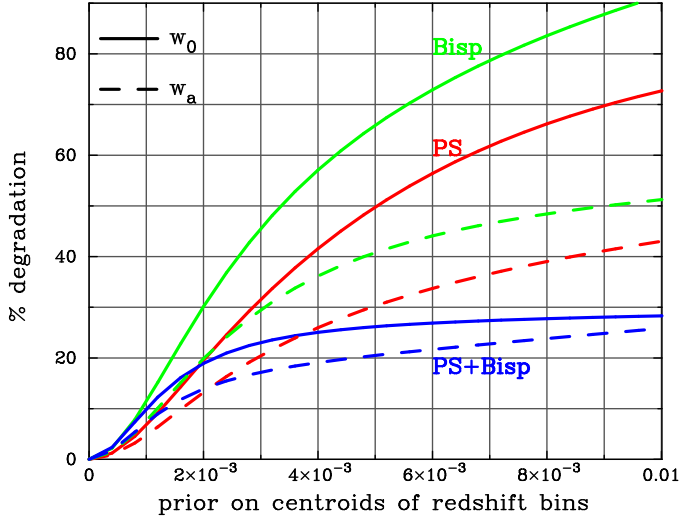


FIG. 12: The centroids of the photometric redshifts must be known to the accuracy of around 0.1% in order to avoid significant degradation of dark energy constraints [71].

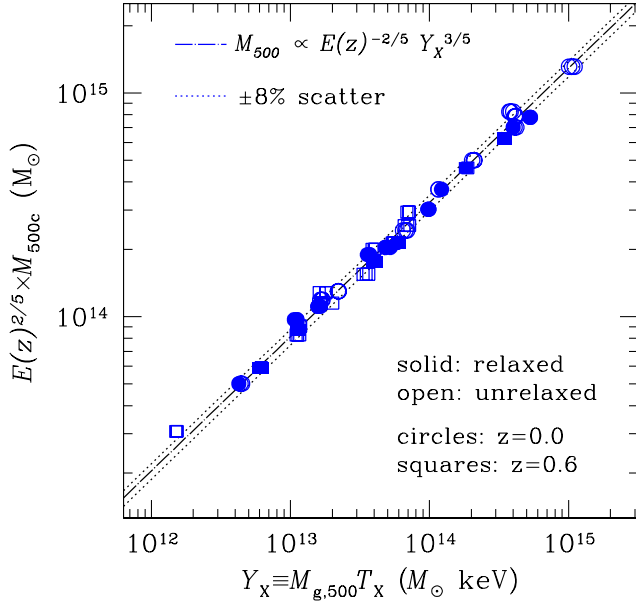


FIG. 13: Total cluster mass versus a proxy based on the total baryon mass and temperature (both of which can be inferred from X-ray observations), based on simulated X-ray data [81].